

Photovoltaic Potential of the Dutch Inland Shipping Fleet

An Experimentally Validated Method to Simulate the Power Series from Vessel-Integrated Photovoltaics

de Jong, Dora ; Ziar, Hesan

DOI

[10.1002/solr.202200642](https://doi.org/10.1002/solr.202200642)

Publication date

2022

Document Version

Final published version

Published in

Solar RRL

Citation (APA)

de Jong, D., & Ziar, H. (2022). Photovoltaic Potential of the Dutch Inland Shipping Fleet: An Experimentally Validated Method to Simulate the Power Series from Vessel-Integrated Photovoltaics. *Solar RRL*, 7 (2023)(8), Article 2200642. <https://doi.org/10.1002/solr.202200642>

Important note

To cite this publication, please use the final published version (if applicable).
Please check the document version above.

Copyright

Other than for strictly personal use, it is not permitted to download, forward or distribute the text or part of it, without the consent of the author(s) and/or copyright holder(s), unless the work is under an open content license such as Creative Commons.

Takedown policy

Please contact us and provide details if you believe this document breaches copyrights.
We will remove access to the work immediately and investigate your claim.

Photovoltaic Potential of the Dutch Inland Shipping Fleet: An Experimentally Validated Method to Simulate the Power Series from Vessel-Integrated Photovoltaics


Dora de Jong and Hesam Ziar*

The surface of the vessels, as moving tiny islands, can be utilized to implement vehicle-integrated photovoltaics (VIPV). Herein, a methodology is reported to calculate the power generated by a fleet of urban vessels as a function of time. Then, the result is shown for the largest European shipping fleet, using sailing data of 2746 Dutch general cargo vessels. Results show that the studied fleet can produce ≈ 226 GWh of energy per year, which corresponds to $\approx 6.5\%$ of the whole fleet's energy demand. Next, this research validates the model with three week experimental data gathered by a test vessel sailing through the Netherlands. The validation phase reveals that the model can predict within a 4% error range. Finally, as an interesting finding, it is experimentally shown that the energy production profile of a fleet of urban vessels follows a Weibull distribution, quantified by scale (λ) and shape (k) parameters: $\lambda = 880 \text{ Wh Wp}^{-1}$ and $k = 27$ for the Dutch fleet. A sensitivity analysis shows that the parameters of the Weibull distribution are a function of urban fabric roughness and the climate. Such probability distribution can be extended to other urban fleets, such as solar cars, and help estimate the financial feasibility of integrating PV into vehicles.

1. Introduction

Despite a drop during the COVID pandemic, the CO₂ emission from transportation has increased again. Globally, transportation emitted 8.5 Gton of CO₂ in 2019,^[1] which accounts for 14% of CO₂ emissions, including water-based transportation.^[2] Water-based transportation emits $\approx 2\%$ of the global CO₂.^[1] Several subsectors of transportation, such as trucks and buses, aviation, and shipping, are not on track with meeting the global targets. Only EVs are growing rapidly but no direct impact on CO₂ reduction has been observed yet^[3] as EVs are charged by grid electricity

D. de Jong, H. Ziar
Photovoltaic Materials and Devices group
Delft University of Technology
2628CD Delft, The Netherlands
E-mail: h.ziar@tudelft.nl

 The ORCID identification number(s) for the author(s) of this article can be found under <https://doi.org/10.1002/solr.202200642>.

© 2022 The Authors. Solar RRL published by Wiley-VCH GmbH. This is an open access article under the terms of the Creative Commons Attribution-NonCommercial-NoDerivs License, which permits use and distribution in any medium, provided the original work is properly cited, the use is non-commercial and no modifications or adaptations are made.

DOI: 10.1002/solr.202200642

that is still dominated by fossil fuels. This imposes the necessity to introduce renewable energy, both in the grid and onboard vehicles, to achieve the actual reduction of CO₂.^[4] Large transportation vehicles, such as trailers and vessels, benefit from relatively large areas, where conventional photovoltaic (PV) technologies can be integrated.^[5–7] Therefore, to make the transportation sector more sustainable, the surface of vessels can also be used for onboard PV module installation.

The Netherlands has the largest fleet in Europe, making up 38.4% of the European shipping fleet.^[8] As the largest European fleet, the Dutch inland shipping industry aims to be climate neutral and emission-free by 2050. To meet this goal, the propulsion of the inland shipping vessels needs to change from diesel-powered to diesel-electric (short term), battery-electric (medium term), and hydrogen-fuel cell (long term).^[9] The inland fleet consists of

5060 vessels, with various types, such as general cargo vessels.^[10] General cargo vessels seem to be suitable for the implementation of PV modules. There are a couple of advantages of these vessel types that make them suitable for the implementation of PV modules. These ships have little equipment installed on top of their deck. General cargo ships have a relatively large surface area that is only used to store goods, the hold, which can be smartly integrated with PV modules (see **Figure 1** as an example). Above this hold, PV modules can be integrated. All ships of this type look similar. The ship is designed as rectangular as possible, to be able to transport as many goods as possible onboard. The wheelhouse is located at the back, before that there is the hold of the vessel. After the vessel's hold, there is a small part that contains the necessary equipment, such as anchors and cranes. From the complete inland shipping fleet, 79% of the vessels are general cargo inland vessels.^[10]

As electric vessels have batteries onboard, one can envision a fleet of urban vessels as a fleet of small PV power plants that supply power to the electrical grid whenever needed. Decentralized energy production will also lower the power losses due to less transmission. The same applies to electric cars or future solar cars.

However, assessing the PV power that a vehicle can produce is challenging.^[11] Unlike a stationary PV plant, modules on a vehicle move around and their ambient and surrounding changes.



Figure 1. A bulk vessel with integrated PV. Photograph courtesy of Wattlab.nl.

For an urban vessel, this is even more challenging as the vibrations due to waves can alter the tilt/orientation angle of PV modules. This effect is more influential on offshore applications, such as offshore floating PV,^[12,13] where the magnitude of waves is several times bigger than inland calm waters. Further, the speed vector of the vessel influences the effective wind and changes the PV module temperature and subsequently power. Studies on vehicle-integrated PV showed that the speed of the vessel should not be neglected when the effective wind speed on the PV module is calculated.^[14] Moreover, the load on a vessel changes its sinking depth and thus installation height of the PV modules alters with respect to the raised horizon around the vessel. This effect is almost unimportant for open seas but should be considered when a vessel is cruising inland, where landscape, buildings, vegetation, etc. are blocking part of the sky dome.

Considering the aforementioned importance of knowing the PV potential of urban ships and pinpointing associated challenges, in this research, we aimed for developing and validating a methodology to simulate the PV power production of vehicle-integrated PV systems at every time step. The rest of this article is organized as follows. **Section 2** describes in detail the methodology, data, and submodules of the model developed in this work. Then, **Section 3** discusses the experimental plan and platform. Further, **Section 4** presents the results of the simulation and experiments. Finally, in **Section 5**, the research results are highlighted.

2. Methodology

A MATLAB-based simulation framework (see **Figure 2**) is developed to simulate the PV power production of vehicle-integrated solar PV systems at predetermined time steps. This simulation framework consists of five subparts: skyline model, vessel model, irradiance model, temperature model, and PV power model.

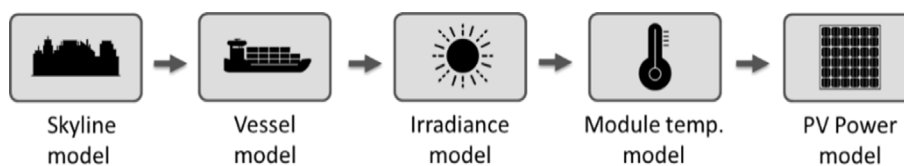


Figure 2. Submodels of the developed MATLAB-based simulation framework.

2.1. Skyline Model

The surrounding of a moving vehicle, in this case a vessel, is changing over time. The skylines of the Dutch waterways represent the changing surrounding of the general cargo vessels sailing over these canals. The skyline model is developed to simulate the surroundings of the Dutch inland shipping waterways. In total, 3036 geo-referenced waterway points provide a representation of the locations of the waterways used by inland shipping vessels (see **Figure 3**). For every waterway data points, a skyline is generated to simulate the surroundings of that location. The waterways points of the Netherlands are provided by the Dutch government, Rijkswaterstaat.^[15] The distance between the points is on average 1000 m. Rijkswaterstaat only provides waterway data points for the canals, not for the lakes and open waters such as IJsselmeer.

Height data of the Netherlands is used to generate a skyline of a specific waterway point. The Dutch government provides a digital surface model (DSM) of the whole Netherlands. Light detecting and ranging (LIDAR) technologies are used to generate this DSM dataset. In this work, the AHN3 (Actueel Hoogtebestand Nederland 3) with a resolution of $0.5 \times 0.5 \text{ m}^2$ is used.^[16] The AHN3 DSM dataset of the complete Netherlands is divided into 1374 tiles. Each tile represents a Tiff image with a size of around 500 MB, which for the whole Netherlands adds up to a complete AHN3 DSM dataset of 656 GB.

The location of the waterway (ww) points in a 3D grid can be denoted by Cartesian coordinates as (x_{ww}, y_{ww}, z_{ww}) . The LIDAR height data of the Netherlands give us information about every point in the sky dome. When considering one point from the AHN dataset, its location can be defined as $(x_{AHN}, y_{AHN}, z_{AHN})$. The altitude and azimuth of this specified point p , with respect to the waterways point, can be calculated using simple geometry by the following equations.

$$r_{ww-AHN} = \sqrt{(x_{AHN} - x_{ww})^2 + (y_{AHN} - y_{ww})^2} \quad (1)$$

$$\theta_{ww-AHN} = \tan^{-1} \left(\frac{y_{AHN} - y_{ww}}{x_{AHN} - x_{ww}} \right) \quad (2)$$

$$\alpha_{ww-AHN} = \tan^{-1} \left(\frac{z_{AHN} - z_{ww}}{r_{ww-AHN}} \right) \quad (3)$$

where θ is the azimuth angle and α is the altitude angle. For every azimuth from 0° to 360° , with a step size of 0.5° , the highest raised altitude (elevation of the vegetation and buildings), observed from the waterway point, is visualized in a skyline profile (see **Figure 4**). The scan radius to generate the skyline at a specific point is considered 1000 m ($r_{ww-AHN,max} = 1000 \text{ m}$).

The skyline is generated from the waterway up. A waterway height of -0.745 is used, which is the average drainage level of the Netherlands waterways, $z_{ww} = -0.745 \text{ m}$. A drainage level



Figure 3. Geo-referenced waterway points of the shipping fleet in the Netherlands, obtained from processed data.

is the water level of the canals with respect to Normaal Amsterdams Peil (NAP).^[17]

The solid angle of the sun is an indication of how large the sun appears to an observer who is located on earth. The sun covers the sky on average with an angular diameter of 0.53° .^[18] Because of the average sun's solid angle, the step size of 0.5° is used for both the altitude and the azimuth.

2.2. Vessel Model

The Vessel model is developed to simulate the different vessels for which the energy yield is calculated. General cargo inland

vessels are usually two types: container vessels and bulk vessels.^[19] For container vessels, the PV modules can be placed on top of the containers while the holds of the bulk vessels are a suitable area to implement PV. The containers have standard sizes and are made to be stacked on top of each other. Therefore, PV modules can be easily connected and systematically placed. Bulk vessels have hatches that cover the holds. PV modules can be installed on the hatches of these vessels. An example of this implementation is given in Figure 1.^[20] The PV modules are placed on top of the holds. The hold is above the waterline and the PV modules are away from the splash zone. As a result, salinization and/or marine deposits will not take place on the PV modules. For a container vessel, the PV modules are installed horizontally. The heading of modules is the same as the heading of the container vessel. On the other hand, for a bulk vessel, PV modules are installed at a tilted angle on both sides of the hatches. The hatches have corridors that must remain free for safety reasons. The average tilt of the hatches is 8° .^[21] The modules installed on the starboard side have an azimuth of the vessel's heading plus 90° , while the PV modules installed on the port side have an azimuth of the vessel's heading plus 90° , as indicated in Figure 5.^[21]

Information about the general cargo vessels can be obtained from AIS data.^[16] AIS data are stored anonymously for every corporate vessel in the Netherlands for every second.^[22] The AIS dataset contains the location, heading, speed, length, and width of all the individual general cargo vessels. The AIS dataset provided by the Dutch government is very large and to some extent disorganized. As the data for the whole year were too large to be provided, this research used the AIS data from 2019 for the months of January, April, July, and October. The year 2019 is chosen as this is the most recent year, while COVID was not interfering with the inland shipping industry. For every hour the vessel location is known from the AIS data. The skyline of the waterway point closest to this vessel's location is assumed

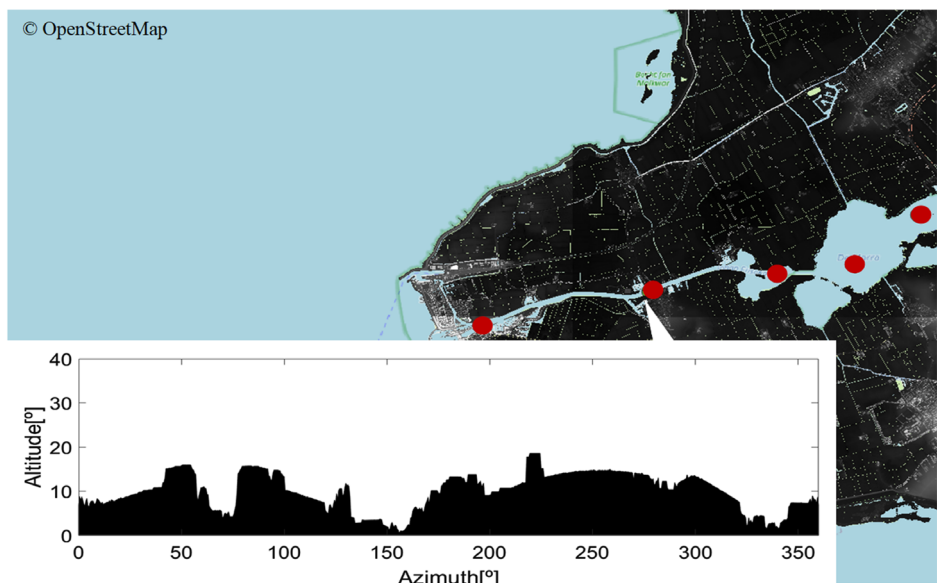


Figure 4. Example of waterway points and an example of extracted surrounding (horizon).

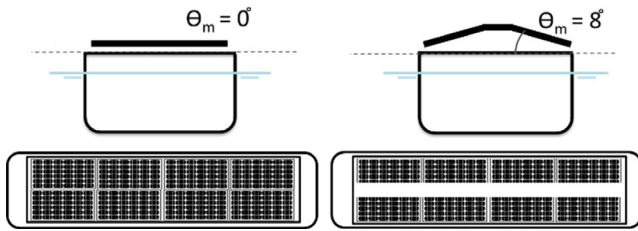


Figure 5. Cross-sectional container (left) and bulk (right) vessel and the PV module installation manner.

to be the vessel skyline. When the vessel is in open waters, a free skyline is considered.

The skylines of the waterways are generated considering the waterlines as the height reference. When a vessel is transporting cargo, the draught of the vessel is higher as the vessel sinks deeper. The height of the vessel's holds depends on the load that the vessel carries. As the vessel sinks into the water, the installation height of the PV modules changes. Therefore, the PV modules' height for skyline extraction should be corrected based on the vessel's load. The draught of a vessel for a specific vessel length, when it is loaded or unloaded, is provided by the governmental organization.^[23] In this model, it is assumed that half of the time the vessel is transporting cargo. The average height of the PV module, when the vessel is loaded and unloaded, is used as an overall height correction on the skyline.

2.3. Irradiance Model

The irradiance model uses climate data as input to simulate the solar irradiance received by the PV modules implemented on the vessels. Climate data are obtained from the nearest KNMI weather station,^[24] depending on the vessel's location. The model retrieves hourly Global Horizontal Irradiance (GHI). Then, Direct Normal Irradiance (DNI) and Diffuse Horizontal Irradiance (DHI) are decomposed from the GHI, according to the irradiance decomposition model of Boland–Redley–Lauret (BRL).^[25]

The irradiance on the PV module, G_{PoA} , is divided into three different components: direct, diffused, and reflected components.^[26]

$$G_{PoA} = G_{dir} + G_{diff} + G_{ground} \quad (4)$$

The direct component of irradiance is a proportion of the DNI, corrected with the angle of incidence (AOI), the angle between the normal of the PV module and the sunlight direction.^[27] If the sun is blocked by the surrounding objects, according to the generated skylines, the PV module will not receive direct irradiance. This effect is modeled by the shading factor (SF), which is unity when the sun is not blocked by its surroundings; otherwise, it is zero.

$$G_{dir} = DNI \cdot \cos(AOI) \cdot SF \quad (5)$$

In this research, the Perez model is used to calculate the diffused component, as this is a sophisticated model that takes hourly climate data into account.^[28] The diffused irradiance is composed of three components.^[27] The first component is the isotropic component, G_{iso} , which indicates the overall irradiance

from the sky dome.^[27] The circumsolar component, G_{cir} , represents the irradiance around the sun disk. The last component is the horizon brightening component, G_{hor} , which models the horizontally diffused irradiance.

$$G_{diff} = DHI \cdot (SVF \cdot (1 - F_1) + F_1 \cdot SF \cdot \left(\frac{A}{B}\right) + F_2 \cdot \sin \theta_m) \quad (6)$$

The three terms in Equation (6), from left to right, are, respectively, G_{iso} , G_{cir} , and G_{hor} . The Perez model calculates the circumsolar and horizon brightening components on complex empirical fitted functions F1 and F2. F1 and F2 can be calculated for a specific sky clearness value.^[29] The equations of F1, F2, A, and B are depicted in **Appendix A**. The sky view factor (SVF) is a factor that indicates the proportion of the sky that is visible by the PV module. The SVF is calculated from the skyline profiles based on the work of D.G. Steyn.^[30]

The ground reflected component is a function of G_h (see Equation (7)). G_h contains the components of irradiance which is received by the earth's surface: the direct irradiance, the circumsolar diffused irradiance, and the isotropic diffused irradiance (see Appendix A). Albedo, the second indicator in Equation (7), represents the reflectivity of the ground. In this research, the water albedo of 0.06 is considered.^[31] VF_{ground} indicates the proportion of the ground from which the module can receive the reflected irradiance.

$$G_{ground} = G_h \cdot \alpha \cdot VF_{ground} \quad (7)$$

2.4. Module Temperature Model

The module temperature has an influence on the performance of the PV module. In this research, the fluid-dynamic model is used as the thermal model.^[27] There are three different cooling mechanisms for a PV module: radiation, convection, and conduction. The conduction coefficient is neglected as a very small area of the PV module has contact with the mounting structure. The PV module radiates heat toward the sky and toward the deck of the vessel. The air movement at the top and back of the PV module cools the module. This is indicated in the heat transfer balance in Equation (B1) in **Appendix B**. The convection on the back side of the PV module is lower compared to the top side of the PV module, as the PV module is mounted on a structure. The convection difference between the top and back sides of the PV module is calculated with the ratio factor R , where R is the ratio between the actual and the ideal heat loss from the back side. The R ratio takes into account the effect of the mounting structure by correcting the nominal operating cell temperature (NOCT). In our simulations, the NOCT is corrected with +18 °C, indicating direct mounting systems.^[27]

The module temperature can be calculated when rewriting the heat transfer balance in Appendix B

$$T_m = \frac{\alpha G + h_{c,top} T_a + h_{c,back} T_a + h_{r,sky} T_{sky} + h_{r,deck} T_{deck}}{h_{c,top} + h_{c,back} + h_{r,sky} + h_{r,deck}} \quad (8)$$

Equation (8) tells how the irradiation G and the ambient temperature T_a affect the module temperature. The wind speed is implemented in the top convective heat transfer coefficients

$h_{c,top}$. The deck temperature T_{deck} is assumed to be the same as the water temperature, for simplicity. The water temperature is also taken into account in the radiative heat coefficients of $h_{r,sky}$ and $h_{r,deck}$. The effect of cloud coverage implemented the temperature of the sky T_{sky} .

When a PV module is installed on a moving body, it is possible that the PV module is cooled more when comparing it to a fixed PV module. The PV module experiences more airflow, caused by the movement of the vessel. This additional cooling effect will decrease the module temperature, which boosts the performance of the module. It is assumed that a body, which is moving at a certain speed, encounters an air flow with the same speed as the moving body. Therefore, the wind speed is corrected with the vessel's velocity with respect to the ground, speed over ground (SOG). The meteorological parameters are again obtained from the nearest KNMI weather station depending on the province the vessel is located.

2.5. PV Power Model (DC Yield Model)

The PV power submodule consists of two parts: the PV module fitting calculator^[32] and the PV power calculator. The former calculates the maximum available area for PV installations on each type and size of the vessel then fits the maximum number of modules, and the latter calculates the output PV power at each timestamp. The submodule needs irradiance, PV module temperature, and specifications. In this research, a monocrystalline Longi PV module LR4-60HPB with a rated power of 360 W was considered.

The PV surface is calculated for every vessel individually and runs simulations for both landscape and portrait orientations, selecting the optimum PV surface utilization. For the container vessels, the PV modules are placed flat, above the containers in the cargo hold. For the bulk vessels, the PV modules are tilted on both sides of the hatches. The flat part of the hatches will not be used for PV installations as this must remain free as a corridor.

Dimensions of the hold for every vessel depend on the vessel's size. AIS data provide the length and width of the vessel but do not provide the dimensions of the holds. The company Blommaert Aluminium Constructions manufactures the hatches for almost all general cargo ships in the Netherlands.^[21] The company has provided, for this research, the relationship between the dimensions of the ships and their hold for four characteristic sizes. General cargo ships are organized in six different classes (CEMT-klassen).^[23] Every class has guidelines for the dimensions of the ships. These guidelines are based on the dimensions of the canals, sluices, and bridges.

As a result, four characteristic ships provide a good indication of the complete fleet. The company also provided the ratio of the corridor width and the average tilt angle of 8° of the hatches. A margin of 0.1 m is considered between the PV modules and the hold edges. The spacing of 0.1 m was decided after a field survey.

The PV power model is based on efficiency calculations and uses the single diode model. The working temperature and irradiance are different from the STC values and that affects the working efficiency. Thus the efficiency must be corrected. This corrected efficiency is indicated in **Appendix C**. By knowing the working efficiency $\eta(T_m, G)$, irradiance G , module temperature T_m , and the number of modules n_m , one can calculate the produced power at every hour

$$P(T_m, G) = \eta(T_m, G) \cdot G \cdot A_m \cdot n_m \quad (9)$$

The PV power in the simulation is calculated for every hour for every vessel individually. For the complete general cargo fleet, the PV power is integrated over 8760 h (see Equation (10)). du indicates a time step of 1 h.

$$E(T_m, G) = \int_{\text{year}} P(T_m, G) du \quad (10)$$

3. Experimental Validation

The developed simulation model was validated by an experiment, whereby a PV module was installed on a test vessel, *Harmonie*. The PV module and the ship were monitored for 3 weeks.

3.1. Experiment Setup

The ship's dimensions are as follows: 10 m in length, 2.85 m in width, and a draught of 0.9 m. The test vessel *Harmonie* is an electrical battery-based propelled by a 22 kW 3-Phase AC asynchronous electrical motor. In a 48 V 800 Ah battery system, energy is stored, which is delivered by shore energy (grid). To perform the experiment, a PV energy system was installed. On the vessel's top deck, a monocrystalline half-cut PERC LR4-60HPB Longi 360 W peak PV module was installed. This PV module is also used in the MATLAB simulation. The module was installed on a structure that enabled various tilts. The mast of *Harmonie* has been lowered during the entire experiment, to prevent shadows on the PV module. The PV module is connected to an EPsolar Tracer 415BN 12/24 V 40 A charger controller, which uses maximum power point tracking (MPPT). The energy that is generated is stored in two lead-acid batteries with a voltage of 12 V and a total capacity of 240 Ah. Four data loggers were installed on *Harmonie*, to store various parameters. To monitor the PV module, a EPEVER eloG01 data logger is connected to the charge controller. A Qstarz BL-1000ST BLE GPS travel recorder and a motion data logger are installed on the PV module. An Alecto WS-5500 wind data logger is installed to monitor the wind speed (see **Figure 6**). **Table 1** lists the data loggers and recorded parameters.

3.2. Travel Route

During the experiment, *Harmonie's* PV module tilt was set to 0°, imitating a container vessel, and 8° toward the port, imitating a bulk vessel. **Appendix D** shows the travel report of the experiment weeks.

During the first week of experimenting, *Harmonie* was docked in a harbor in the center of Rotterdam (see the red dot in **Figure 7**). The harbor of Rotterdam is the biggest harbor in the Netherlands. This port was specifically chosen as it is located in an urban area of Rotterdam. Therefore, the effect of obstructed horizon on the PV energy yield can be analyzed. **Appendix E** shows the horizon around the harbor point.

During the second and third weeks, *Harmonie* followed its scheduled route through the Netherlands. **Figure 7** shows the

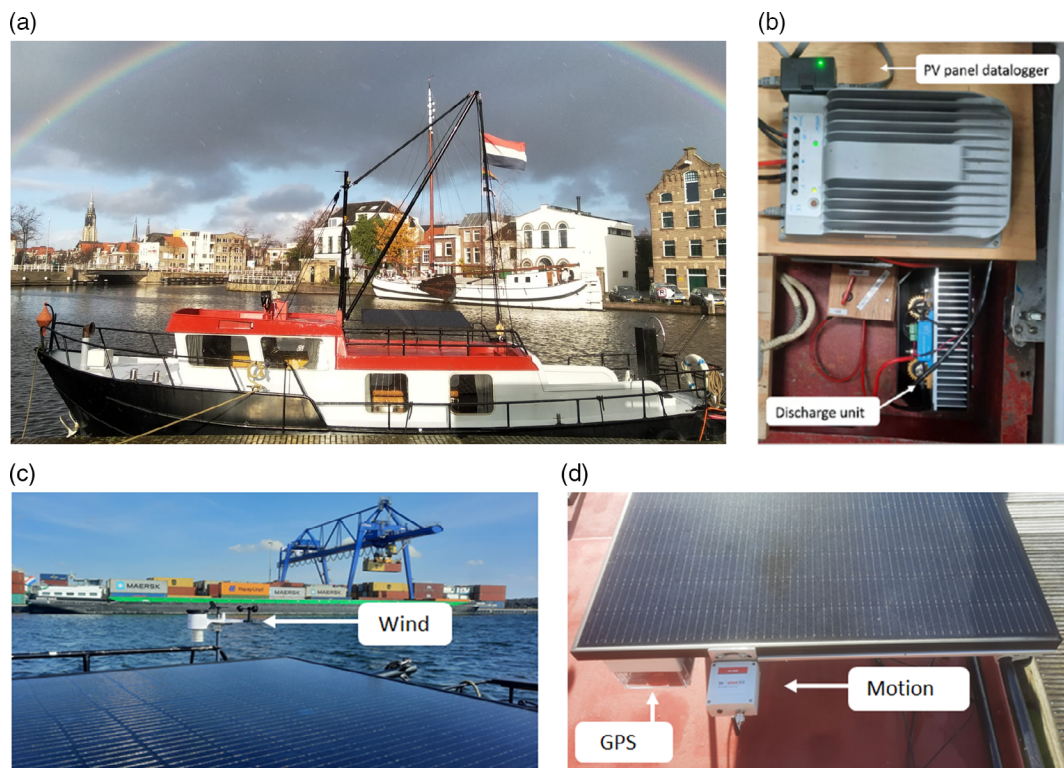


Figure 6. Experimental test setup. a) The test vessel Harmonie at a port in Delft, the Netherlands. b) Charge controller, PV panel data logger, and the battery discharge system and its protection unit. c) PV module and the wind sensor. d) PV module, GPS, and motion sensor.

Table 1. Data loggers and recorded data information.

Data logger	Stored parameter	Time interval	Accuracy
PV module	Module DC power, voltage, current	10 min	Unknown
Wind	Wind speed	5 min	$\pm 1 \text{ m s}^{-1} > 5 \text{ m s}^{-1}$ and $\pm 10\% < 5 \text{ m s}^{-1}$
GPS	Location, heading, speed	5 min	Speed: $\pm 0.05 \text{ m/s}$
Motion	Pitch and roll motions, ambient temperature	30 s	Motion: $0.03\% < 5^\circ$ and 0.17% full range Temp.: $\pm 0.5^\circ$

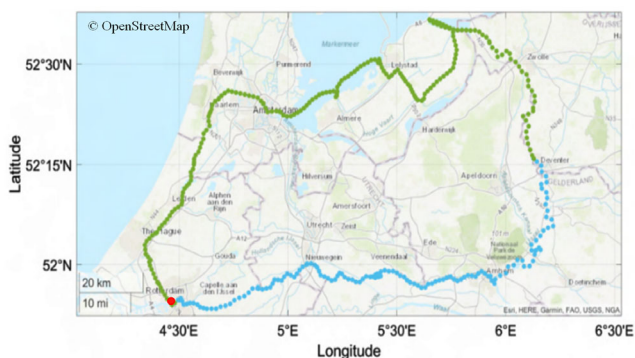


Figure 7. Sailing route of the test vessel Harmonie.

sailed route. For blue, green, and red dots, the module tilt was, respectively, 8° , 0° , and 8° . This sailing route has been mapped out in such a way that Harmonie sails in different directions and sails in different types of waters. Harmonie followed four main

and busy canals and also has crossed the largest open inland waters of the Netherlands, the IJsselmeer and Markermeer. There were two break days in the two sailing weeks, during which no measurements were done. During the two sailing weeks, the Harmonie sailed for 63 h and 20 min, on average $\approx 5 \text{ h day}^{-1}$. The Harmonie always sailed during the daytime and most of the time between 12:00 and 17:00.

3.3. Experiment Outcomes and Statistical Analysis

The roll motion (here equivalent to module tilt) of Harmonie varied $\pm 1.09^\circ$ and $\pm 3.0^\circ$ when the vessel was docked and sailing, respectively. The pitch motion (here equivalent to module azimuth) when Harmonie was docked and sailing varied $\pm 2.71^\circ$ and $\pm 9.38^\circ$, respectively (see Appendix F).

The PV energy yield and the energy demand for the two sailing weeks have been measured. Most of the energy demand comes from the consumption of the engine. Figure 8 shows the power

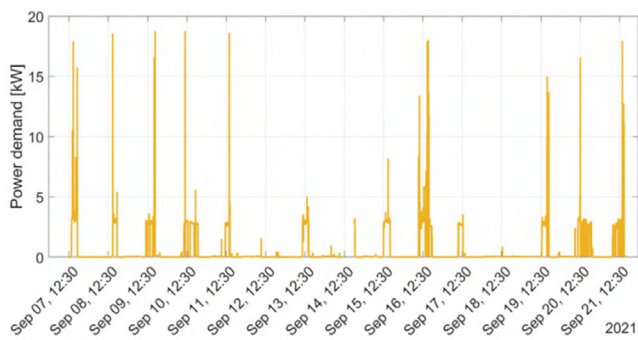


Figure 8. Power demand of the Harmonie's engine.

demand of the engine of the Harmonie. On September 12 and 18, the energy demand is almost zero, as the Harmonie did not sail. The total energy demand of the Harmonie was 162 kWh and the PV energy generation was 11 kWh. Thus, 6.60% of the energy demand was supplied by the PV module and the rest was from shore power. The 6.60% of the energy demand coverage by PV is only from one PV module. The Harmonie would have the capacity to integrate 4 PV modules. The Harmonie is a recreational vessel, and on holidays the vessel would not have the same sailing pattern as during the experiment, which will result in a higher percentage of energy demand that can be covered with PV energy.

To validate the developed model, a covariance linear regression model is used. The regression model describes the relationship between the measured data, response, and different predictors. The linear regression model is given by

$$\text{Measured} = \alpha \times \text{Estimated} + \beta \times \text{Sailing} + \gamma \times \text{Tilt} \quad (11)$$

where Measured is a response variable that contains 170 measured PV power values; Estimated is a predictor variable which contains 170 values of the estimated PV power; Sailing is a binary predictor variable, which is 1 when the vessel is sailing; and Tilt is a binary predictor variable, where 1 indicates if the PV module is tilted 8° to the port side. **Table 2** shows the regression coefficients α , β , and γ with the corresponding p -values.

The significance level of the model is set to 5%, 0.05. We studied the p -values for each predictor to understand the importance of each predictor: model estimations, sailing, and module tilt. The p -value for the predictor value Estimated is below the significance level, indicating that there is a relation between the measured and estimated PV power. The α is 0.96; therefore, the model overestimates the outcomes by 4%. The R^2 of the linear regression model is 0.70. The simulation model is able to estimate the outcomes close to the measured values. **Figure 9** shows the linear regression model, the 170 data points, and the ideal line where the estimated values are equal to the measured values.

Table 2. The covariance linear regression model.

	Coefficients	p -value	95% confidence interval
Estimated	$\alpha = 0.96$	2.43×10^{-48}	[0.87 1.05]
Sailing	$\beta = -2.08$	0.65	[-11.14 6.97]
Tilt	$\gamma = 8.56$	0.03	[0.97 16.15]

The Sailing predictor has a p -value above 0.05, which indicates that the prediction of the model is not affected by the sailing or docking status of the vessel. The Tilt predictor is statistically significant; the effect of a different tilt on the outcome of the measured PV power is not random, as the p -value is below 0.05. As the Tilt is a binary vector and gamma is 8.56, the measured outcome can be affected by 8.56 W for a tilt of 8° compared to a tilt of 0°. The effect of 8.56 W is relatively small as the PV power range is between 0 and 230 W.

4. Results

Now that we are confident the model provides accurate results, we follow with modeling the whole fleet. In this research, 2746 general cargo vessels are considered in the developed simulation model, of which 2146 bulk vessels and 600 container vessels.

4.1. Sailing Behavior

The sailing behavior of the general cargo vessels is an important factor when determining the PV energy yield of the fleet. From the data, we extracted the probability a general cargo vessel is sailing during an average day (**Figure 10**). Between 08:30 and 16:30, the probability that a vessel is sailing is the highest. The probability at night is only slightly lower, a sufficient amount of vessels still sail at night. A cargo vessel sails on average for 48.68% of the time.

Appendix G shows how the waterway points are scattered throughout the whole country, and how often a vessel passes through every waterway point. According to the AIS dataset, the vessels sail fairly uniformly through the Dutch waterways, with the exception of the ports. The traffic is higher near the Rotterdam and Amsterdam ports, thus the amount of clean PV energy that could be generated by the fleet is higher at those locations. The ports in Rotterdam and Amsterdam are the biggest ports in the Netherlands.

4.2. Surroundings of the Dutch Waterways

The horizon for 3036 waterway points throughout the whole Netherlands was obtained and analyzed. It was found that the average values of SVFs for vessels sailing through the Dutch waterway points was 95%. The maximum SVF for the container and bulk vessels is 1 and 0.9951, respectively. The equation $[(1 + \cos(8^\circ))/2]$ confirms that the SVF of 0.9951 is the theoretical maximum of a PV module titled 8°, with an open horizon. The minimum SVF for the container and bulk vessels is 0.0051 and 0.0049. This occurs when a vessel is sailing under a bridge or through a lock.

4.3. Surface Utilization

The suitable surface for PV modules on the general cargo inland vessels is calculated for every vessel individually. This is an important parameter used to estimate the PV potential of the Dutch general cargo fleet. The total PV surface of the complete general cargo fleet is 1 359 794 m² (see **Table 3**). The PV surface on average for a general cargo inland vessel is 495.19 m².

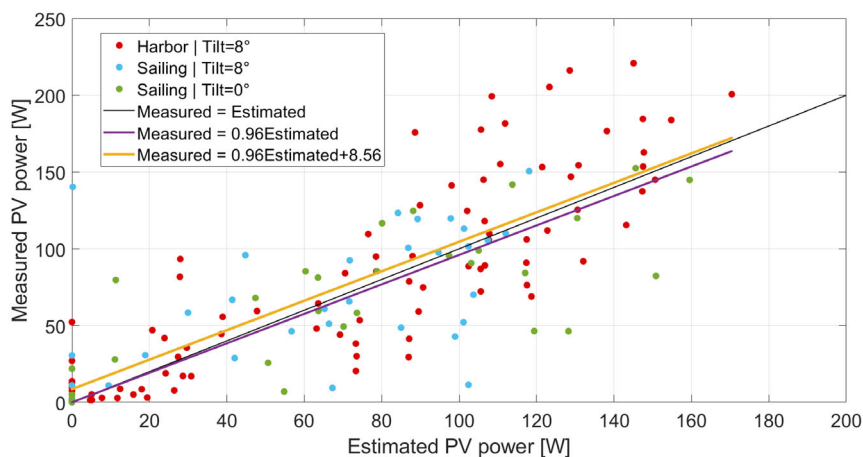


Figure 9. Measured data points and the results of the covariance linear regression model.

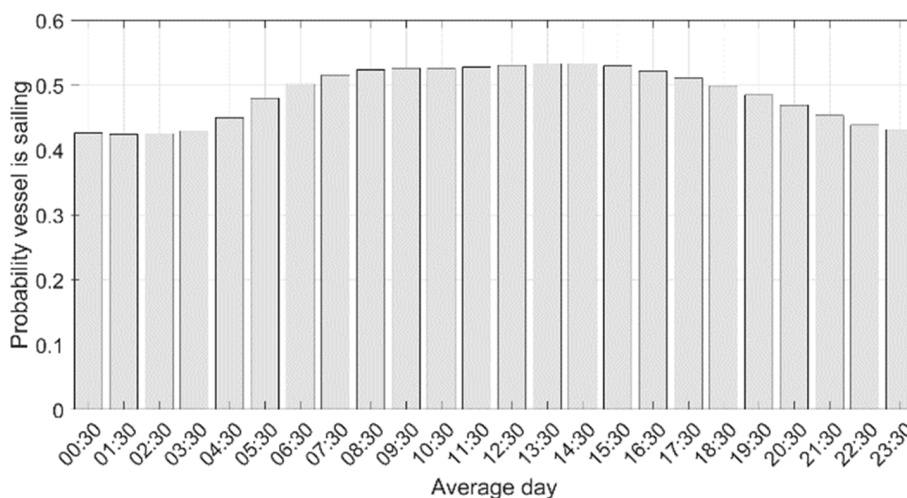


Figure 10. Sailing behavior over an average day.

Table 3. Overview of PV module placement capacity for the fleet.

	Container vessels	Bulk vessels	General cargo fleet
Number of vessels	600	2146	2746
Mean PV surface area [m ²]	599.45	461.38	495.19
Total PV surface area [m ²]	369 670	990 124	1 359 794
Mean PV surface utilization [%]	60.49	50.83	52.94
Mean PV installed power [kWp]	118.46	91.18	97.14
Total PV installed power [MWp]	71.08	195.67	266.75
Mean number of installed modules	329.06	253.27	269.83
Total number of installed modules	197 438	543 520	740 958

We defined PV surface utilization as the percentage of suitable PV surface with respect to the vessel's surface. The surface utilization of an average container and bulk vessel is 60.49% and 50.83%, respectively. For bulk vessels, the PV modules are installed on the hatches of the holds, which contain a corridor

and therefore have a smaller average PV surface utilization. There might be other surfaces on a vessel, such as the wall, windows and roofs of the cabin, or even the outside body of the ship. Due to curvature or the need for light to pass through, these spots can be covered by thin film and/or transparent PV. However, usually such surfaces do not have favorable angle toward the sky which limits their energy production.

As mentioned in Section 2.5, 360 Wp PV modules were used in the simulation. The total installed peak power on the general cargo fleet is 266.74 MWp, which comprises 740 958 installed PV modules. On an average general cargo vessel, 270 modules can be installed. Table 3 gives an overview of the potential PV surface area, PV installed peak power, and the number of installed modules.

4.4. Photovoltaic Energy Yield

Table 4 gives an overview of the potential PV energy of the container and bulk vessels and the whole fleet combined. The simulated PV energy yield gives an estimation of the PV energy potential of the general cargo fleet. The average annual PV energy

Table 4. Annual PV energy yield calculated for the fleet.

	Container vessels	Bulk vessels	General cargo fleet
Mean annual PV energy yield per unit area [kWh m^{-2}]	169.42	166.67	167.27
Total annual PV energy yield [GWh]	58.30	167.33	225.63
Mean annual PV energy yield [MWh]	103.37	77.97	83.52
Max annual PV energy yield [MWh]	825.35	1724.80	1724.80
Min annual PV energy yield [MWh]	2.96	175.65	2.96
Specific PV energy yield [kWh kWp^{-1}]	857.31	843.39	861.39
Max specific PV energy yield [kWh kWp^{-1}]	939.63	929.50	939.63
Min specific PV energy yield [kWh kWp^{-1}]	76.92	7.82	7.82

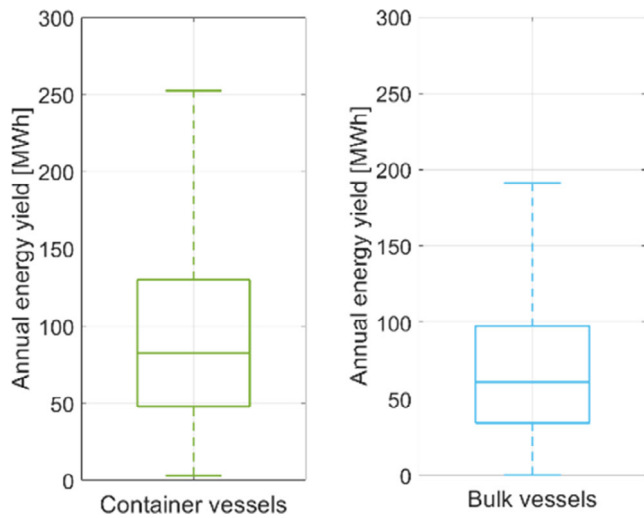


Figure 11. Annual energy yield distribution for the container and bulk vessels.

potential per area is $167.27 \text{ kWh m}^{-2}$. The energy per unit area for a container vessel is $169.42 \text{ kWh m}^{-2}$ and for a bulk vessel $166.67 \text{ kWh m}^{-2}$. According to these values, placing a PV module flat is on average slightly more effective than tilting them angle of 8° to the port and starboard sides.

Figure 11 shows a box plot of the annual energy yield distribution for the container and bulk vessel. The total annual energy generated when installing PV modules on general cargo vessels is 225.63 GWh. Comparing this generated energy with the energy needed to produce the installed PV modules on the general cargo vessels, the Energy PayBack Time on average is 7 years and 15 days.^[33] On average, the annual energy yield of the container and bulk vessels is 103.37 and 77.97 MWh, respectively. The minimum generated annual energy yield for container vessels is 2.96 MWh which is relatively small compared to the 175.65 MWh for the bulk vessel. This annual PV energy is related to a small surface area of a container vessel, i.e., 30 m^2 . This vessel is 34 m in length and 3 m in width.

Figure 12 shows the distribution of the monthly PV energy per unit area for the general cargo vessels. December and January have the lowest energy generation per unit area and May and June are the highest.

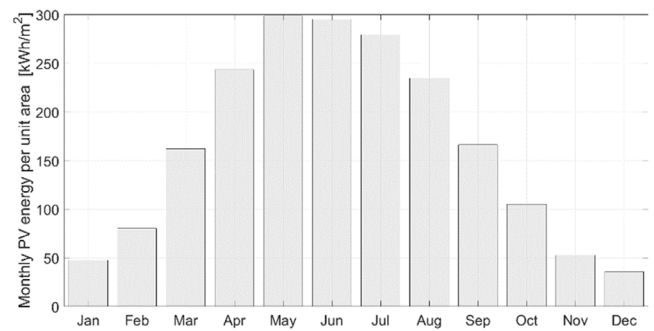


Figure 12. Monthly PV energy per unit area for the general cargo vessels.

4.5. Energy Demand

The energy demand of a general cargo vessel depends on its size. The typical engine power for every size class of general cargo vessel is provided by the Rijkswaterstaat.^[23] The annual energy demand of a 110 m inland shipping vessel, according to the research of Panthei, is 2500 MWh.^[9] This number is cross-validated in a conversation with an inland shipping vessel expert of the Delft University of Technology, Dr. ir. H.J. de Koning Gans.^[34] The average energy demand of a general cargo vessel, for a specified length class, can be calculated by scaling the energy demand of 2500 MWh with the engine power of the different general cargo size classes.

This energy demand can then be compared with energy generated by PV on the vessels. For container vessels, the average annual energy demand is 1440 MWh and the annual PV generation is 103 MWh, as indicated in Table 4. This generated energy can cover 7.18% of the energy demand. The average energy demand of a bulk vessel is 1350 MWh and the average energy generated by the PV modules is 78 MWh; thus, 5.78% of the energy demand can be supplied by PV energy. Note that these values will increase when in the future more ships will use electric propulsion with higher efficiencies.

4.6. Energy Distribution of Fleet

Probability distributions emerging from studying a fleet of PV systems have already attracted attention.^[35] We continued our study with analyzing the probability distribution of the

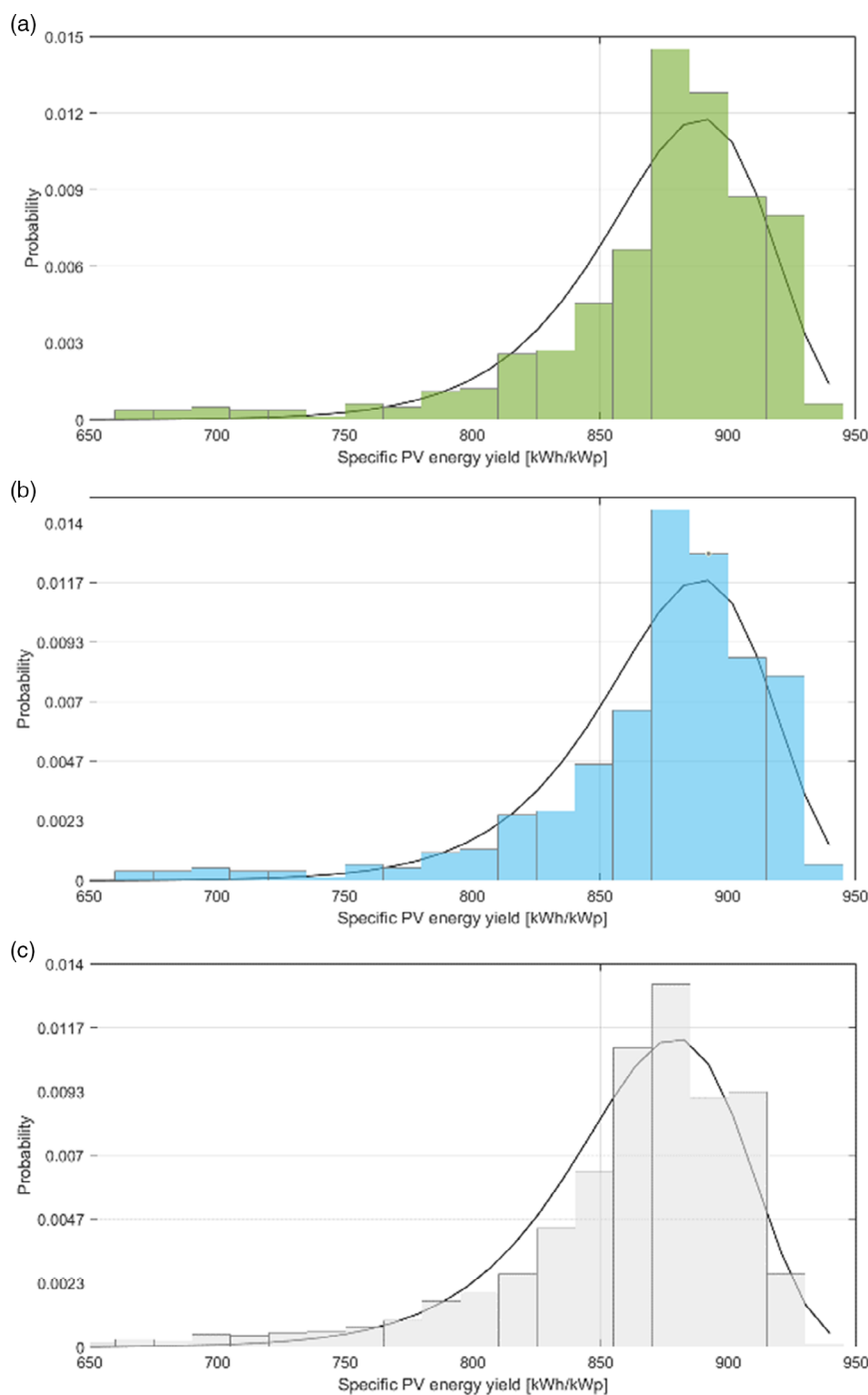


Figure 13. Weibull distribution of the Dutch urban fleet: a) container vessels ($\lambda = 890.64 \text{ Wh Wp}^{-1}$, $\kappa = 28.54$); b) bulk vessels ($\lambda = 877.31 \text{ Wh Wp}^{-1}$, $\kappa = 27.20$); and c) the whole general cargo fleet ($\lambda = 880.30 \text{ Wh Wp}^{-1}$, $\kappa = 26.99$). Note that κ is dimensionless while λ has the same unit as the x axis.

specific energy yield of the vessel's fleet. The general cargo vessels that transport containers on average can generate $857.31 \text{ Wh Wp}^{-1}$. Bulk vessels will generate less; they have a smaller PV surface utilization and thus less specific PV energy yield, $843.39 \text{ Wh Wp}^{-1}$. For the whole cargo fleet, the average energy per installed power over a year is $861.39 \text{ Wh Wp}^{-1}$. Table 4 gives an overview of the potential PV energy per installed power.

For further research, it is useful to know the probability distribution of the PV energy generation of the general cargo vessel. A probability distribution fit is perused by studying 17 different continuous distributions. For every probability distribution, four statistical weighting factors are calculated and compared: NLogL (negative of the log-likelihood), BIC (Bayesian information criterion), AIC (Akaike information criterion), and AICc

(Akaike information criterion for small sample size).^[36] These factors examine the goodness of the fit for a specific probability distribution.

The best fitting probability function for the specific annual PV energy is the t location-scale distribution. Usually, in statistics, the t location-scale distribution is used for smaller datasets with heavier tails, containing more outliers.^[37] When removing the outliers out of the data set the best distribution fit changes to a Weibull distribution, according to the same 17 possible continuous distributions and the four statistic weighting factors. It is indeed interesting as previous literature did also report on fitting Weibull distribution to irradiance data.^[38–41] Plots in **Figure 13** show the Weibull distribution for container vessels, bulk vessels, and the whole fleet. Equation (12) gives the continuous probability function when the scale and shape factors are larger than zero.

$$f(x, \lambda, \kappa) = \frac{\kappa}{\lambda} \left(\frac{x}{\lambda}\right)^{\kappa-1} e^{-\left(\frac{x}{\lambda}\right)^\kappa} \quad (12)$$

where $\kappa > 0$ is the shape parameter and $\lambda > 0$ is the scale parameter. Statistical analysis of the simulation outcome showed $\lambda = 891 \text{ Wh Wp}^{-1}$ and $k = 28.54$ for container vessels and $\lambda = 877 \text{ Wh Wp}^{-1}$ and $k = 27.20$ for bulk vessels.

A sensitivity analysis on the probability distribution showed that the parameters of Weibull distribution are mainly linked to the city roughness and climate. In inner city parts, where the horizon is more blocked, the Weibull distribution shifts to the left and its peak flattens (lower λ , higher κ) while in the countryside with fewer obstacles on the horizon, the Weibull distribution shifts to the right and its peak increases (higher λ , lower κ). Therefore, the roughness of urban fabric (r) works as a shifter smoother on the Weibull distribution ($d\lambda/dr < 0$, $d\kappa/dr > 0$). Further, our analysis showed that vehicles movement speed (assuming inner city speed ranges) has minor effect on the Weibull distribution parameters. By testing different fleet populations, we found that the larger the fleet size, the better is the fit with the Weibull distribution.

4.7. Computational Time

Generating a skyline of the surrounding is a time-consuming process, which significantly lowers the simulation speed. Therefore, the skyline model is developed, which generates skylines of the waterways. Instead of generating skylines for every vessel at every time step, a database of waterway skylines was developed. This allows large-scale implementations of vessels; in this research, the biggest fleet in Europe is implemented.

The computational time for a container vessel is 1:18 min. The computational time for a bulk vessel is 2 times bigger. The simulation for a bulk vessel needs to run 2 times, as two PV systems with different azimuths are installed on both sides of the hatches. With a personal laptop, the total computational time of the general cargo inland shipping fleet is 4 days and 10:30 h.

5. Conclusions

The objective of this research was to establish a modeling framework for the simulation of vehicle-integrated PV s. This was accomplished by determining the PV potential of the largest

European general cargo fleet, the Dutch. This is of great importance especially for countries with low land accessibility for energy production purposes. The surface utilization of a container vessel is 60% and for a bulk vessel is 51%. The total potential surface area of the general cargo inland fleet that can be used to integrate PV systems is 1.36 km^2 .

The developed simulation model is an irradiance model framework that estimates the energy yield from hourly power calculations. With LIDAR height data, a dataset of skyline profiles for 3036 waterway points was generated. The average sky view factor of the general cargo vessels is 0.945. By the means of AIS data, the sailing behavior of 2746 general cargo vessels was simulated. On an average 24 h day, a general cargo vessel is sailing 51% of the time. The irradiance model uses the BRL decomposition model to decompose the DNI and DHI from the GHI. The diffused irradiance is calculated based on the Perez model. The PV module temperature is estimated according to the fluid-dynamic model, taking into account the additional air caused by the movement of the vessel and the water temperature.

The PV power is calculated according to a single diode model.

Three weeks of measurements with a test vessel were conducted to validate the simulation framework. According to the covariance linear regression model, the simulated PV power series for this experiment is statistically significant and overestimated the PV power by 4% with a 95% confidence interval between 0.87 and 1.05.

The estimated annual PV energy potential of the general cargo fleet is 226 GWh. The specific annual PV energy yield for a container vessel is 857 Wh Wp^{-1} and for a bulk vessel is 843 Wh Wp^{-1} . The probability distribution functions which can describe the annual PV energy per peak power are the t location-scale and the Weibull distribution if the outliers are considered and removed, respectively. Our results showed that 7.18% and 5.78% of the energy demand of container and bulk vessels, respectively, can be supplied by implementing PV modules on general cargo vessels.

Appendix A. Irradiance calculations

Irradiance on the surface of the PV module (G_{PoA}) can be modeled by the following main equation.

$$G_{PoA} = G_{dir} + G_{diff} + G_{ground} \quad (A1)$$

where G_{dir} , G_{diff} , and G_{ground} , respectively, stand for the direct, diffuse, and ground reflected components of the sunlight irradiance.

A.1. Direct Irradiance

Direct part of the irradiance, the part that directly reaches to the target surface from the sun disk, can be obtained by

$$G_{dir} = DNI \cdot \cos(\text{AOI}) \cdot SF \quad (A2)$$

where

$$\cos(\text{AOI}) = \sin(\theta_m) \cos(\alpha_s) + \cos(A_m - A_s) + \cos(\theta_m) \sin(\alpha_s) \quad (A3)$$

and

$$SF = \begin{cases} 0 & \text{when the sun is blocked} \\ 1 & \text{when the sun is not blocked} \end{cases} \quad (\text{A4})$$

In Equation (A2)–(A4), DNI is the direct normal irradiance (W m^{-2}), AOI stands for the angle of incidence, and SF is the shading factor. θ_m , α_s , A_m , and A_s angles are, respectively, PV module tilt, altitude angle of the sun, azimuth angles of the module, and the sun.

A.2. Diffused Irradiance

The diffuse component is subdivided into three parts: isotropic (G_{iso}), circumsolar (G_{cir}), and horizon brightening (G_{hor})

$$G_{\text{diff}} = G_{\text{iso}} + G_{\text{cir}} + G_{\text{hor}} \quad (\text{A5})$$

where

$$G_{\text{iso}} = \text{DHI} \cdot \text{SVF} \cdot (1 - F_1) \quad (\text{A6})$$

and

$$G_{\text{cir}} = \text{DHI} \cdot F_1 \cdot (A/B) \cdot SF \quad (\text{A7})$$

$$A/B = \max(0, \cos(AOI)) / \max(\cos(85), \sin(\alpha_s)) \quad (\text{A8})$$

and

$$G_{\text{hor}} = \text{DHI} \cdot F_2 \cdot \sin(\theta_m) \quad (\text{A9})$$

In Equation (A6)–(A9), DHI is the diffuse horizontal irradiance (W m^{-2}) and SVF is the sky view factor. Factors F_1 , F_2 , A , and B are determined using the following set of equations

$$F_1 = \max \left[0, \left(f_{11} + f_{12}\Delta + \frac{\pi\theta_z}{180^\circ} f_{13} \right) \right] \quad (\text{A10})$$

$$F_2 = f_{21} + f_{22}\Delta + \frac{\pi\theta_z}{180^\circ} f_{23} \quad (\text{A11})$$

$$\Delta = \frac{\text{DHI} \times \text{AM}_a}{E_a} \quad (\text{A12})$$

$$\varepsilon = \frac{\kappa\theta_z^2 + (\text{DHI} + \text{DNI})/\text{DHI}}{1 + \kappa\theta_z^2} \quad (\text{A13})$$

$$E_a = E_{sc} \times \left(\frac{R_{av}}{R} \right)^2 \quad (\text{A14})$$

$$\left(\frac{R_{av}}{R} \right) = (1.00011 + 0.034221 \cos(b) + 0.00128 \sin(b) + 0.000719 \cos(2b) + 0.000077 \sin(2b)) \quad (\text{A15})$$

$$b = 2\pi \frac{\text{DOY}}{365} \quad (\text{A16})$$

where θ_z is the solar zenith angle, E_a is the extraterrestrial radiation which is the sun radiation intensity at the top of the atmosphere, and E_{sc} is the solar constant (1367 W m^{-2}). κ is a constant equal to 1.041 when angles are in radians or equal to 5.535×10^{-6} when angles are in degrees. AM_a is the absolute

Table A1. Perez model coefficients for irradiance.

ε_{bin}	f_{11}	f_{12}	f_{13}	f_{21}	f_{22}	f_{23}
1	−0.008	0.588	−0.062	−0.06	0.072	−0.022
2	0.13	0.683	−0.151	−0.019	0.066	−0.029
3	0.33	0.487	−0.221	0.055	−0.064	−0.026
4	0.568	0.187	−0.295	0.109	−0.152	−0.014
5	0.873	−0.392	−0.362	0.226	−0.462	0.001
6	1.132	−1.237	−0.412	0.288	−0.823	0.056
7	1.06	−1.6	−0.359	0.264	−1.127	0.131
8	0.678	−0.327	−0.25	0.156	−1.377	0.251

air mass and ε is related to the cloud coverage (okta) and defines the bins for the f coefficients, as shown in **Table A1**. R_{av} is the average distance between the sun and the earth while R is the distance between the sun and the earth and a specific time. Finally, DOY is an integer number representing the day of the year.

A.3. Ground Reflected Irradiance

The part of irradiance reflected from the ground (G_{ground}) and falling on the PV module is obtained by knowing the albedo of the ground (α_{ground}) and the view factor from the module to the ground ($\text{VF}_{\text{ground}}$)

$$G_{\text{ground}} = G_h \cdot \alpha_{\text{albedo}} \cdot \text{VF}_{\text{ground}} \quad (\text{A17})$$

where

$$G_h = (\text{DNI} \cdot \sin(\alpha_s) \cdot SF) + G_{\text{iso}} + G_{\text{cir}} \quad (\text{A18})$$

and

$$\alpha_{\text{albedo}} = 0.06 \quad (\text{A19})$$

$$\text{VF}_{\text{ground}} = (1 - \cos(\theta_m))/2 \quad (\text{A20})$$

As the material covering the ground, in this case, is the water which has a low albedo, the value of 6% was considered.

Appendix B. Heat transfer balance

Considering the PV module as a single mass with uniform temperature T_m and placed in ambient with the temperature of T_a that works under steady state condition (i.e., the module temperature does not change within the duration of one time step), one can write the heat transfer balance equation as follows

$$q_{\text{sun}} = q_{\text{rad,deck}} + q_{\text{rad,sky}} + q_{\text{conv,top}} + q_{\text{conv,back}} \quad (\text{B1})$$

where q_{sun} is the heat received from the sun in the form of irradiance; $q_{\text{rad,deck}}$ and $q_{\text{rad,sky}}$ are the heat radiated from the module, respectively, toward the sky and deck of the vessel; $q_{\text{conv,top}}$ and $q_{\text{conv,back}}$ are representing the heat transfer via convection from the top and back side of the PV module. In Equation (B1), the contribution of conduction in heat transfer is neglected due

to the small contact area between the PV and the vessel's deck. The equation can be further simplified as follows

$$\alpha G = h_{c,top}(T_m - T_a) + h_{c,back}(T_m - T_a) + h_{r,deck}(T_m - T_{deck}) + h_{r,sky}(T_m - T_{sky}) \quad (B2)$$

where T_{sky} and T_{deck} stand for the temperature of the sky and the vessels' deck, respectively. G is the irradiance falling on the module and here α is the absorptivity of the PV module. $h_{c,top}$ and $h_{c,back}$ are the convective heat transfer coefficients, respectively, for the front and rear sides of the PV module.

The other two coefficients can be found by

$$h_{r,deck} = \epsilon_{back} \sigma (T_m^2 + T_{deck}^2)(T_m + T_{deck}) \quad (B3)$$

$$h_{r,sky} = \epsilon_{top} \sigma (T_m^2 + T_{sky}^2)(T_m + T_{sky}) \quad (B4)$$

where ϵ_{back} and ϵ_{top} are the emissivity of the PV panel from the back and the top part of the PV panel, respectively. σ is the Stefan–Boltzmann constant.

Appendix C. Photovoltaic power and energy calculations

Using the following set of equations, one can obtain the PV module efficiency at a non-STC condition, $\eta(T_m, G)$, by knowing the datasheet efficiency, $\eta(STC)$, and assuming a constant fill factor (FF).

n is a ideality factor of 1.2

$$P(T_m, G) = \eta(T_m, G) \cdot G \cdot A_m \cdot n_m \quad (C1)$$

$$E(T_m, G) = \int_{year} P(T_m, G, u) du \quad (C2)$$

$$\eta(T_m, G) = \eta(25^\circ C, G) \left[1 + \left(\frac{1}{\eta(STC)} \frac{\partial \eta}{\partial T} \right) (T_m - 25^\circ C) \right] \quad (C3)$$

$$\eta(25^\circ C, G) = \frac{FF \cdot V_{OC}(25^\circ C, G) I_{SC}(25^\circ C, G)}{G \cdot A_m} \quad (C4)$$

$$V_{OC}(25^\circ C, G) = V_{OC}(STC) + \frac{nk_B T_m}{q} \ln \left(\frac{G}{1000} \right) \quad (C5)$$

$$I_{SC}(25^\circ C, G) = I_{SC}(STC) \frac{G}{1000} \quad (C6)$$

$$FF = \frac{P_{mpp}}{V_{OC}(STC) I_{SC}(STC)} \quad (C7)$$

In Equation (C1)–(C7), n is the ideality factor (in this work considered as 1.2) and k_B is the Boltzmann constant. V_{OC} , I_{SC} , and P_{mpp} are, respectively, open-circuit voltage, short-circuit current, and the maximum power point of the PV module. We note that in equation (C5), the T_m , module temperature, can be plugged in Kelvin, yet in the others are in Celsius.

Appendix D. Travel report

Day	Date	Start time	End time	Sailing duration [h:min]	Start location	End location	Module tilt [°]
1	7/9/2021	13:47	17:37	3:50	Rotterdam	Schoonhoven	8
2	8/9/2021	15:17	17:47	2:30	Schoonhoven	Nieuwegein	8
3	9/9/2021	11:27	16:27	5:00	Nieuwegein	Wijk bij duurstede	8
4	10/9/2021	10:47	18:57	8:10	Wijk bij duurstede	Arnhem	8
5	11/9/2021	11:57	14:37	2:40	Arnhem	Frankerwaard	8
6	12/9/2021				Break		
7	13/9/2021	11:07	14:47	3:40	Frankerwaard	Deventer	8
8	14/9/2021	14:19	18:59	4:40	Deventer	Kampen	0
9	15/9/2021	12:29	16:19	3:50	Kampen	Ketelhaven	0
10	16/9/2021	10:19	17:59	7:40	Ketelhaven	Lelystad	0
11	17/9/2021	10:09	12:49	2:40	Lelystad	Almere	0
12	18/9/2021				Break		
13	19/9/2021	13:09	17:19	4:10	Almere	Amsterdam	0
14	20/9/2021	11:19	19:19	8:00	Amsterdam	Leiden	0
15	21/9/2021	08:29	14:59	6:30	Leiden	Rotterdam	0

Times are local (Central Europe time).

Appendix E. Skyline of the Harmonie when docked in the harbor of Rotterdam (Figure E1)

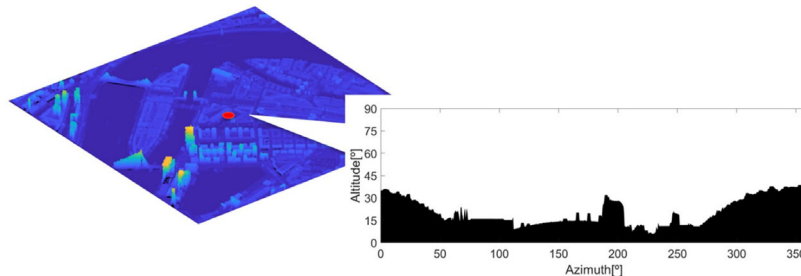


Figure E1. Digital surface map and the skyline of the harbor around the test vessel when it was docked at the red point.

**Appendix F. Motion data from the experiment
(Figure F1 and F2)**

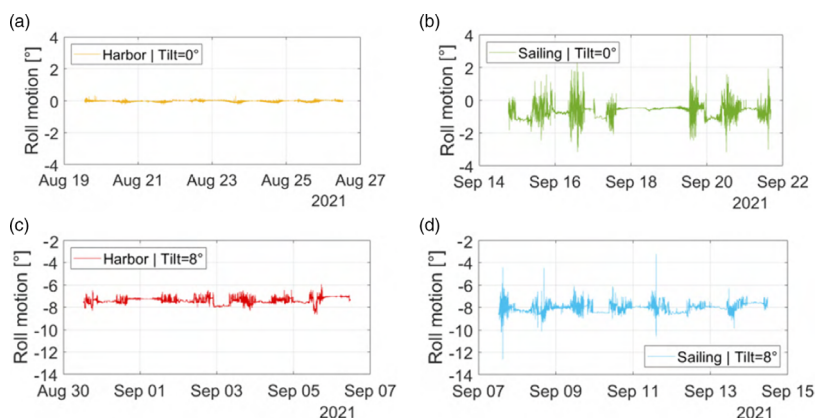


Figure F1. Logged roll angle of the PV panel, equivalent to module tilt, under four different conditions: a) docked at the harbor with 0° tilt, b) cruising with 0° tilt, c) docked at the harbor with 8° tilt, and d) cruising with 8° tilt.

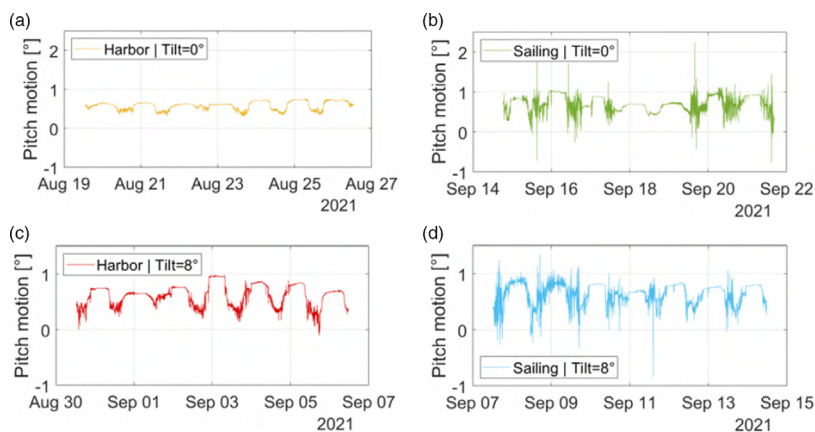


Figure F2. Logged pitch angle, equivalent to module azimuth, of the PV panel at four different conditions: a) docked at the harbor with 0° tilt, b) cruising with 0° tilt, c) docked at the harbor with 8° tilt, and d) cruising with 8° tilt.

Appendix G. Traffic of the main Dutch canals by general cargo vessels (Figure G1)

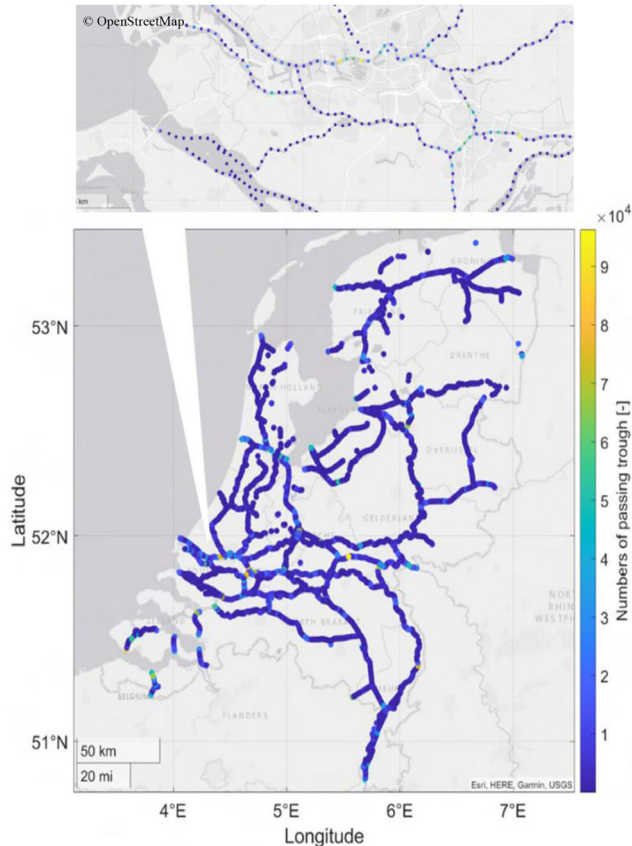


Figure G1. (Bottom) Traffic map of the general cargo vessel for the Dutch waterways obtained from the AIS data. (Top) The zoomed-in area of the Rotterdam harbor. Considering future general cargo fleets equipped with PV and acting as small moving PV plants, the map can be seen also as the geographical PV potential density of the Dutch general cargo fleet.

Acknowledgements

The authors are thankful for the help from Ms. Solange van der Werff for assistance in retrieving AIS data. The authors are grateful to the scientific support of Ms. Vasiliki Sionti for providing the sensitivity analysis results on the Weibull probability distribution with respect to vehicle speed, fleet population, and city roughness. The authors would like to thank Mr. Stefaan Heirmann for assembling the battery protect unit and technical support on the power train of the test vessel.

Conflict of Interest

The authors declare no conflict of interest.

Data Availability Statement

The data that support the findings of this study are available from the corresponding author upon reasonable request.

Keywords

ships, solar photovoltaic potential, vehicle-integrated photovoltaics (VIPV), waterways, urban area

Received: July 15, 2022
Revised: August 31, 2022
Published online: October 3, 2022

- [1] IEA, International Shipping, Paris **2021**, <https://www.iea.org/reports/international-shipping> (accessed: June 2022).
- [2] SLOCAT Partnership on Suitable, Low Carbon Transport, Global Transport and Climate Change **2022**, <https://tcc-gsr.com/global-overview/global-transport-and-climate-change/>, (Geopend 2022).
- [3] G. Rizzo, M. Naddeo, C. Pisanti, *Int. J. Powertrains* **2018**, 7, 249.
- [4] A. Abas, J. Yong, J. Yong, T. Mahlia, M. Hannan, *IEEE Access* **2019**, 7, 98565.
- [5] A. Vulpe, C. Lupu, C. Mihai, S. Dan, in *Int. Symp. Fundamentals of Elect. Eng. (ISFEE)*, IEEE, Bucharest, Romania **2018**.
- [6] Kutter, Christoph, F. Basler, L. E. Alanis, J. Markert, H. Martin, D. H. Neuhaus, presented at 37th Europ. PV Solar Energy Conf. and Exhib., September 2020.
- [7] V. Alfonsín, A. Suarez, A. Cancela, A. Sanches, R. Maceiras, *Int. J. Hydrogen Energy* **2014**, 22, 11763.
- [8] CCR, in *Europese Binnenvaart Marktobservatie Jaarverslag 2019*, Centrale Commissie voor de Rijnvaart, Netherlands **2019**.
- [9] Panteia, in *Middellange Termijn Prognoses voor de binnenvaart Vervoer in relatie tot Nederland, periode 2020 - 2025*, Panteia, Netherlands **2020**.
- [10] IVR, in *Scheepsdata nederlandse binnenvaart vloot*, Internationale Vereniging het Rijnschepenregister, Netherlands **2020**.
- [11] Hongda Liu, Q. Zhang, X. Qi, Y. Han, F. Lu, *Appl. Energy* **2017**, 204, 362.
- [12] K. C. Su, P. H. Chung, R. Y. Yang, *J. Mech.* **2021**, 37, 53.
- [13] H. Ziar, *10 Breakthrough Ideas in Energy for the Next 10 Years*, Global Energy Association **2021**, pp. 30–43, https://globalenergyprize.org/en/wp-content/uploads/2021/06/10Ideas_ENG.pdf.
- [14] F. A. Tiano, G. Rizzo, M. Marino, A. Monetti, *eTransportation* **2020**, 5, 100067.
- [15] Rijkswaterstaat, *Dataset: Nationaal Wegen Bestand 2020*.
- [16] Rijkswaterstaat, *Dataset: Actueel Hoogtebestand Nederland 2021*.
- [17] Hoogheemraadschap, *Het juiste waterpeil kiezen? 2020*.
- [18] Swinburne University of Technology, *Swinburne Astronomy Online 2021*.
- [19] Bureau Voorlichting Binnenvaart, *Bureau Voorlichting Binnenvaart 2018*.
- [20] Solar magazine, *Oleander eerste Nederlandse binnenvaartschip met luik van zonnepanelen, 2020*.
- [21] Blommaert, *Friesche kap luiken 2021*.
- [22] International Maritime Organization, *AIS Transponders 2019*.
- [23] Rijkswaterstaat, *Richtlijnen Vaarwegen 2020*, Rijkswaterstaat, Netherlands **2020**.
- [24] Royal Netherlands Meteorological Institute, KNMI Data Platform. <https://dataplatform.knmi.nl/dataset/waarneemstations-3> (accessed: December 2021).
- [25] J. Boland, J. Huang, B. Ridley, *Renewable Sustainable Energy Rev.* **2013**, 28, 749.
- [26] PVPIC, *Plane of Array (POA) Irradiance 2018*.
- [27] A. H. M. Smets, K. Jager, O. Isabella, R. A. C. M. M. van Swaaij, M. Zeman, *Solar Energy*, UIT Cambridge, England **2016**.
- [28] R. Perez, R. Stewart, R. Seals, T. Guertin, *The Development and Verification of the Perez Diffuse Radiation Model*, United States, State University of New York, New York **1988**.
- [29] PVsyst, *Transposition Model 2021*.

- [30] D. G. Steyn, *Res. Note* **1980**, *18*, 254.
- [31] H. Ziar, B. Prudon, F.-Y. Lin, B. Roeffen, D. Heijkoop, T. Stark, S. Teurlincx, L. de Senerpont Domis, E. G. Goma, J. G. Extebarria, I. N. Alavez, D. van Tilborg, H. van Laar, R. Santbergen, O. Isabella, *Prog. Photovoltaics Res. Appl.* **2020**, *29*, 725.
- [32] T. N. d. Vries, J. Bronkhorst, M. Vermeer, J. C. Donker, A. S. Briels, H. Ziar, M. Zeman, O. Isabella, *Sol. Energy* **2020**, *209*, 96.
- [33] L. Beatriz Dai-Prá, J. Batista Dias, A. Gonçalves Kieling, *J. Power Energy Eng.* **2015**, *9*, 592.
- [34] H. de Koning Gans, *Interviewee, Expert in Ship Hydromechanics and Structures at Delft University of Technology*. September **2021**.
- [35] J. Taylor, L. Jonathan, A. M. Everard, J. Briggs, A. Buckley, in *Monitoring Thousands of Distributed PV Systems in the UK: Energy Production and Performance*, PVSAT-11, Leeds, April 2015.
- [36] Y. Aminov, *FBD - "Find the Best Distribution" Tool* **2021**.
- [37] MathWorks, *Location-Scale Distribution* **2021**.
- [38] O. M. Kam, S. Noël, H. Ramenah, P. Kasser, C. Tanougast, *Renewable Energy* **2021**, *165*, 194.
- [39] M. E. Ghitany, N. F. El-Nashar, *Int. J. Sustainable Energy* **2005**, *24*, 167.
- [40] L. Garbai, Z. Kovacs, *Int. Rev. Appl. Sci. Eng.* **2021**, *1*, <https://doi.org/10.1556/1848.2021.00344>.
- [41] M. U. Afzaal, I. A. Sajjad, A. B. Awan, K. N. Paracha, M. F. Khan, A. R. Bhatti, I. Tlili, *Sustainability* **2020**, *12*, 2241.